Production of ^{266}Bh in the ^{248}Cm(^{23}Na,5n)^{266}Bh reaction and its decay properties

H. Haba,[1,*] F. Fan,[2] D. Kaji,[1] Y. Kasamatsu,[3] H. Kikunaga,[4] Y. Komori,[1] N. Kondo,[3] H. Kudo,[5] K. Morimoto,[1] K. Morita,[1,6] M. Murakami,[7] K. Nishio,[8] J. P. Omtvedt,[9] K. Ooe,[10] Z. Qin,[2] D. Sato,[5] N. Sato,[1] T. K. Sato,[8] Y. Shigekawa,[1] A. Shinohara,[3] M. Takeyama,[11] T. Tanaka,[12] A. Toyoshima,[13] K. Tsukada,[8] Y. Wakabayashi,[14] Y. Wang,[1] S. Wulff,[9] S. Yamaki,[1] S. Yano,[1] Y. Yasuda,[3] and T. Yokokita[1]

[1]*Nishina Center for Accelerator-Based Science, RIKEN, Wako, Saitama 351-0198, Japan*
[2]*Institute of Modern Physics, Chinese Academy of Sciences, Lanzhou 730000, China*
[3]*Graduate School of Science, Osaka University, Toyonaka, Osaka 560-0043, Japan*
[4]*Research Center for Electron Photon Science, Tohoku University, Sendai, Miyagi 982-0826, Japan*
[5]*Department of Chemistry, Niigata University, Niigata, Niigata 950-2181, Japan*
[6]*Department of Physics, Kyushu University, Fukuoka 819-0395, Japan*
[7]*Decommissioning and Radioactive Waste Management Head Office, Japan Atomic Energy Agency, Tokai, Ibaraki 319-1112, Japan*
[8]*Advanced Science Research Center, Japan Atomic Energy Agency, Tokai, Ibaraki 319-1195, Japan*
[9]*Department of Chemistry, University of Oslo, 0315 Oslo, Norway*
[10]*Graduate School of Medicine, Osaka University, Suita, Osaka 565-0871, Japan*
[11]*Faculty of Science, Yamagata University, Yamagata 990-8560, Japan*
[12]*Department of Nuclear Physics, Research School of Physics, The Australian National University, Canberra, Australian Capital Territory 2601, Australia*
[13]*Institute for Radiation Sciences, Osaka University, Toyonaka, Osaka 560-0043, Japan*
[14]*Center for Advanced Photonics, RIKEN, Wako, Saitama 351-0198, Japan*

(Received 11 June 2020; accepted 30 July 2020; published 27 August 2020)

The nuclide ^{266}Bh was produced in the ^{248}Cm(^{23}Na,5n)^{266}Bh reaction at beam energies of 125.9, 130.6, and 135.3 MeV. Decay properties of ^{266}Bh were investigated with a rotating wheel apparatus for α and spontaneous fission (SF) spectrometry under low background conditions attained by a gas-jet transport system coupled to the RIKEN gas-filled recoil ion separator. Based on genetically correlated α-α and α-SF decay chains, a total of 23 chains were assigned to ^{266}Bh and its daughter nuclide ^{262}Db and granddaughter ^{258}Lr. The half-life of ^{266}Bh was measured to be $T_{1/2} = 10.0^{+2.6}_{-1.7}$ s which is an order of magnitude longer than the literature data. The α-particle energies of ^{266}Bh disperse widely in the range of $E_\alpha = 8.62$–9.40 MeV. The maximum production cross section for the ^{248}Cm(^{23}Na,5n)^{266}Bh reaction was determined to be $\sigma = 57 \pm 14$ pb at 130.6 MeV, whereas the upper limit for the ^{248}Cm(^{23}Na,4n)^{267}Bh reaction was $\sigma \leqslant 14$ pb at 121.2 MeV. These cross sections are discussed by comparing with the literature data as well as the theoretical calculations.

DOI: 10.1103/PhysRevC.102.024625

I. INTRODUCTION

Decay properties of superheavy element (atomic number $Z \geqslant 104$) nuclei have been systematically investigated to verify the predicted spherical nuclear shell closure at proton number $Z = 114$, 120–126, and neutron number $N = 184$ as well as the deformed shell at $Z = 108$ and $N = 162$ [1–4]. Neutron-rich and long-lived isotopes of ^{267}Bh and ^{266}Bh, which are located around $Z = 108$ and $N = 162$, were first produced by Wilk *et al.* [5] in the ^{249}Bk(^{22}Ne,4n)^{267}Bh and ^{249}Bk(^{22}Ne,5n)^{266}Bh reactions, respectively, at the Lawrence Berkeley National Laboratory 88-in. cyclotron using a gas-jet coupled rotating wheel apparatus which was equipped with six pairs of passivated ion-implanted planar silicon (PIPS) detectors for α spectrometry. Identifications of ^{267}Bh and ^{266}Bh were performed by observation of genetically correlated α decays between the Bh isotopes and their Db and Lr daughter nuclides. Five α-α correlations including one random of unrelated α decays were assigned to ^{267}Bh. ^{267}Bh decays with a half-life $T_{1/2} = 17^{+14}_{-6}$ s by emission of α particles with an average energy of $E_\alpha = 8.83 \pm 0.03$ MeV. Their experimental setup was not sensitive to a spontaneous fission (SF) decay due to fission contamination attributed to ^{256}Fm. The production cross sections for the ^{249}Bk(^{22}Ne,4n)^{267}Bh reaction were $\sigma = 58^{+33}_{-15}$ and 96^{+55}_{-25} pb at 117 and 123 MeV, respectively. At 123 MeV, one α-α-α correlation of ^{266}Bh was observed with $\sigma = 25$–250 pb, decaying within 1 s by emission of a 9.29-MeV α particle. Immediately after the report of the long-lived ^{267}Bh by Wilk *et al.* [5], Eichler *et al.* [6] investigated chemical properties of Bh in the form of its oxychloride where six correlated decay chains of ^{267}Bh (about 1.4 random correlations), formed in the ^{249}Bk(^{22}Ne,4n)^{267}Bh

*haba@riken.jp

TABLE I. Decay properties and production cross sections of ^{266}Bh. Listed are beam energies ($E_{\rm Beam}$), numbers of observed atoms (N), random numbers ($N_{\rm R}$), half-lives ($T_{1/2}$), and cross sections (σ).

Reaction[a]	$E_{\rm Beam}$ (MeV)	$N(N_{\rm R})$	$T_{1/2}$ (s)	E_α (MeV)	σ (pb)	Reference
^{249}Bk(^{22}Ne,5n)^{266}Bh	123	1 (0.0016)	∼1	9.29	25–250	[5]
^{209}Bi(^{70}Zn,n)^{278}Nh → ^{274}Rg → ^{270}Mt → ^{266}Bh	349–351	3 (0.090)	$2.1^{+2.9}_{-0.8}$	9.08; 9.77; 9.39	$0.022^{+0.020}_{-0.013}$	[7–9]
^{243}Am(^{26}Mg,3n)^{266}Bh	135	4 (0.054)	$0.66^{+0.59}_{-0.26}$	9.03 ± 0.08	15 ± 10	[10]
^{248}Cm(^{23}Na,5n)^{266}Bh	126–132	20[b] (0.056)		8.82; 8.84–8.99; 9.05–9.23	50[c]	[11]

[a]Arrows indicate the α-decay chain.
[b]Nine in 20 events were tentative assignments.
[c]Energy-averaged and inclusive cross section of ^{266}Bh and ^{267}Bh

reaction at 119 MeV, were observed with the stepwise rotating wheel equipped with 12 pairs of the PIPS detectors after the chemical separation. The measured six α energies of ^{267}Bh ranged from E_α = 8.72 to 8.91 MeV and the half-life of ^{267}Bh deduced from the average decay time was $T_{1/2} = 14^{+9}_{-4}$ s.

In the new element search program at RIKEN, Wako, Japan, Morita and co-workers [7–9] observed three α decays of ^{266}Bh as a descendant of the element 113 isotope, ^{278}Nh produced in the ^{209}Bi(^{70}Zn,n)^{278}Nh reaction using a silicon semiconductor detector box placed at the focal plane of the RIKEN gas-filled recoil ion separator (GARIS). The reported three α energies of ^{266}Bh ($E_\alpha = 9.08 \pm 0.04$ MeV [7], 9.77 ± 0.04 MeV [8], and 9.39 ± 0.06 MeV [9]) were different from each other and the mean lifetime of the three decays was $\tau = 3.0^{+4.2}_{-1.1}$ s ($T_{1/2} = 2.1^{+2.9}_{-0.8}$ s). The 9.08-MeV α group reported by Morita *et al.* [7] was confirmed in the ^{243}Am(^{26}Mg,3n)^{266}Bh reaction at 135 MeV at the Heavy Ion Research Facility in Lanzhou, China where Qin *et al.* [10] observed four correlated α decays between ^{266}Bh and its daughters ^{262}Db and ^{258}Lr using the rotating wheel system equipped with four pairs of the PIPS detectors. The measured α energy and half-life of ^{266}Bh were $E_\alpha = 9.03 \pm 0.08$ MeV and $T_{1/2} = 0.66^{+0.59}_{-0.26}$ s, respectively. Their experimental setup was not sensitive to the α-SF correlations.

To enhance the decay data of ^{266}Bh, Morita *et al.* [11] studied the decay properties of ^{266}Bh in the ^{248}Cm(^{23}Na,5n)^{266}Bh reaction at 126, 130, and 132 MeV by using the similar experimental setup for the ^{209}Bi(^{70}Zn,n)^{278}Nh reaction [7–9]. The four α-α-α, five α-α, and four α-SF correlations, which initiated from the parent α decays with E_α = 8.82, 8.84, and 9.05–9.23 MeV, were assigned to ^{266}Bh, even though the α energies of E_α = 8.82 and 8.84 MeV just coincide with E_α = 8.83 MeV reported for ^{267}Bh in Ref. [5]. Furthermore, Morita *et al.* [11] tentatively assigned the eight α-SF correlations with a new α group of E_α = 8.93–8.99 MeV for ^{266}Bh. As for ^{267}Bh, one α-α-SF correlation could be assigned to the chain ^{267}Bh → ^{263}Db → ^{259}Lr →. The four α-SF correlations with E_α = 8.71–8.84 MeV, however, were tentatively assigned to ^{267}Bh → ^{263}Db → because the possible assignment to ^{266}Bh → ^{262}Db → could not be excluded due to the very similar decay properties of their daughter nuclides. Since Morita *et al.* [11] analyzed only the data collected in the beam-off period due to high count rates of the focal plane detector of GARIS during the beam-on period, no time difference between the evaporation residue implantation and its decay was obtained. Thus, the half-lives of ^{266}Bh and ^{267}Bh could not be determined. An energy-averaged and inclusive cross section for the ^{248}Cm(^{23}Na,5n)^{266}Bh and ^{248}Cm(^{23}Na,4n)^{267}Bh reactions was σ = 50 pb at 126–132 MeV.

The number of the observed events, half-lives, α energies, and cross sections of ^{266}Bh and ^{267}Bh from the previous studies [5–11] are summarized in Tables I and II, respectively. The α energies and half-lives reported for ^{266}Bh in Refs. [5,7–11] are not in good agreement. The assignments of the observed decay events to ^{266}Bh and ^{267}Bh were often ambiguous due to the very similar decay properties of their daughters ^{262}Db ($T_{1/2}$ = 33.8 s; decay branch $b_\alpha/b_{\rm SF}$ = 48%/52%; E_α = 8.46 and 8.68 MeV [12]) and ^{263}Db ($T_{1/2}$ = 27 s; $b_\alpha/b_{\rm SF}/b_{\rm EC}$ = 41%/55%/3%; E_α = 8.36 MeV [13]), and their granddaughters ^{258}Lr ($T_{1/2}$ = 3.54 s; $b_\alpha/b_{\rm EC}$ = 97.4%/2.6% [12]; E_α = 8.654, 8.621, 8.595, and 8.565 MeV [14]) and ^{259}Lr ($T_{1/2}$ = 6.3 s; $b_\alpha/b_{\rm SF}$ = 77%/23%; E_α = 8.45 MeV [14]). The decay patterns of ^{266}Bh and ^{267}Bh are shown in Fig. 1. In addition, no excitation functions were measured for both the ^{249}Bk(^{22}Ne,5;4n)^{266,267}Bh and ^{248}Cm(^{23}Na,5;4n)^{266,267}Bh

TABLE II. Decay properties and production cross sections of ^{267}Bh. Listed are beam energies ($E_{\rm Beam}$), numbers of observed atoms (N), random numbers ($N_{\rm R}$), half-lives ($T_{1/2}$), and cross sections (σ).

Reaction	$E_{\rm Beam}$ (MeV)	N ($N_{\rm R}$)	$T_{1/2}$ (s)	E_α (MeV)	σ (pb)	Reference
^{249}Bk(^{22}Ne,4n)^{267}Bh	117; 123	3; 2 (∼1)	17^{+14}_{-6}	8.83 ± 0.03	58^{+33}_{-15}; 96^{+55}_{-25}	[5]
^{249}Bk(^{22}Ne,4n)^{267}Bh	119	6 (1.4)	14^{+9}_{-4}[b]	8.72–8.91		[6]
^{248}Cm(^{23}Na,4n)^{267}Bh	126–132	5[a] (0.014)		8.71–8.84	50[c]	[11]

[a]Four events in five were tentative assignments.
[b]The half-life was deduced from the reported lifetimes in Ref. [6] by the authors.
[c]Energy-averaged and inclusive cross section of ^{266}Bh and ^{267}Bh

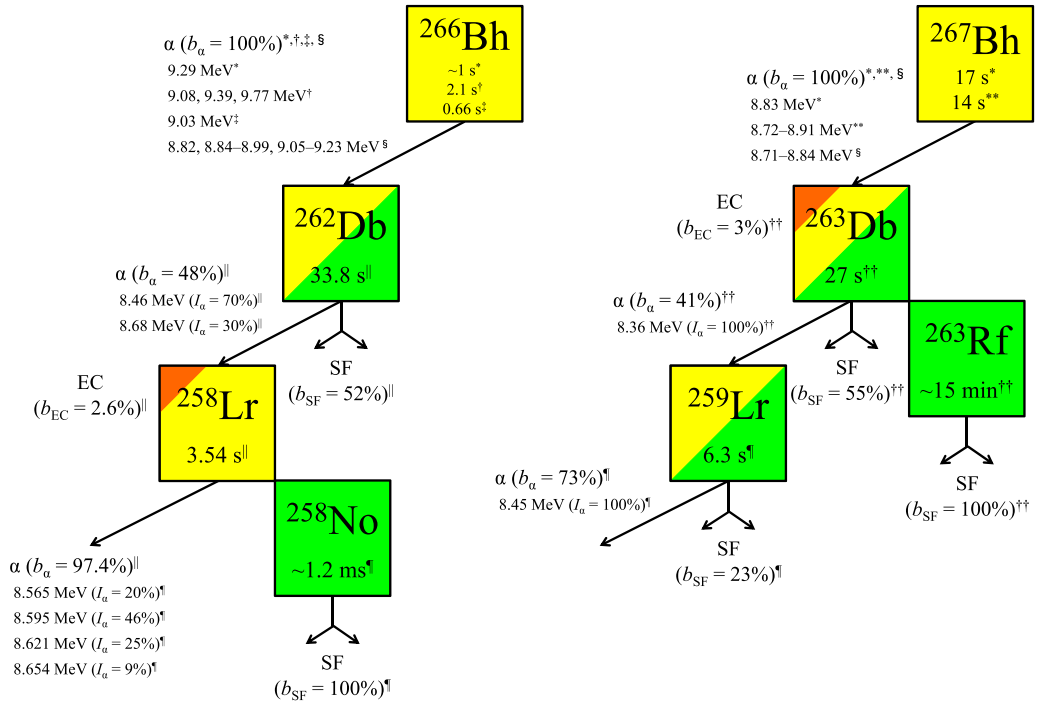

FIG. 1. Decay patterns reported for the chains ^{266}Bh → ^{262}Db → ^{258}Lr → (*: [5]; †: [7–9]; ‡: [10]; §: [11]; ‖: [12]; ¶: [14]) and ^{267}Bh → ^{263}Db → ^{259}Lr → (*: [5]; **: [6]; §: [11]; ††: [13]; ¶: [14]). The electron capture (EC) decay branches are known for ^{258}Lr and ^{263}Db, and their EC decay daughters ^{258}No and ^{263}Rf, respectively, decay by SF.

reactions, although they must be important clue for mass assignments.

The production and decay data of ^{266}Bh as well as ^{267}Bh are still inadequate as mentioned above. This has led us to further studies of the isotopes with use of a more sensitive technique. We have been developing a gas-jet transport system coupled to RIKEN GARIS for use in experimental studies in the field of superheavy element chemistry [15]. ^{261}Rf^{a,b}, ^{262}Db, and ^{265}Sg^{a,b} produced in the ^{248}Cm(^{18}O,5n)^{261}Rf^{a,b}, ^{248}Cm(^{19}F,5n)^{262}Db, and ^{248}Cm(^{22}Ne,5n)^{265}Sg^{a,b} reactions, respectively, were extracted by the gas-jet transport system to a chemistry laboratory after the separation by GARIS [12,16–18]. The α and SF decays of those isotopes were investigated in detail using the measurement system for the α-particle and spontaneous fission events on line (MANON) coupled to the gas-jet transport system under low background conditions. In this paper, we investigated the production and decay properties of ^{266}Bh and ^{267}Bh *via* the ^{248}Cm(^{23}Na,5n)^{266}Bh and ^{248}Cm(^{23}Na,4n)^{267}Bh reactions, respectively, using the GARIS gas-jet and MANON setups.

II. EXPERIMENTAL TECHNIQUES

The experimental conditions, such as beam energy at the middle of the target, thickness of ^{248}Cm target, beam integral, and step interval of MANON, are summarized in Table III. The ^{23}Na^{7+} ion beam was extracted from the RIKEN Linear Accelerator. The ^{248}Cm$_2$O$_3$ targets of 256–290-μg/cm^2 thicknesses were prepared by the molecular-plating method and deposited on a 2-μm Ti backing foil. The isotopic

TABLE III. Experimental conditions and number of correlations. Listed are beam energies, thicknesses of the ^{248}Cm$_2$O$_3$ target, beam integrals, step intervals of the rotating wheel apparatus MANON, and numbers of observed and expected α-α, α-α-α, and α-SF correlations.

Beam energy	Thickness of the ^{248}Cm$_2$O$_3$ target	Beam integral	Step interval of MANON	Number of observed correlations (Expected number of random correlations)		
(MeV)	(μg/cm^2)	($\times 10^{18}$)	(s)	α-α	α-α-α	α-SF
121.2	257	10.20	8.5	0 (0.15)	0 (0.00)	0 (0.02)
125.9	256	9.26	8.5	1 (0.16)	0 (0.00)	3 (0.03)
130.6	290	4.96	5.0	0 (0.16)	0 (0.00)	4 (0.02)
130.6	290	3.99	15.0	5 (0.23)	1 (0.00)	1 (0.01)
130.6	257	8.90	8.5	5 (0.28)	1 (0.00)	3 (0.06)
130.7	257	9.02	8.5	11 (0.43)	3 (0.00)	2 (0.03)
135.3	256	11.21	8.5	9 (0.15)	2 (0.00)	0 (0.02)

composition of the Cm target was 96.64% ^{248}Cm, 0.04% ^{247}Cm, 3.17% ^{246}Cm, 0.13% ^{245}Cm, and 0.02% ^{244}Cm. The eight arc-shaped targets were mounted on a rotating wheel of 100-mm diameter, and the wheel was rotated during the irradiation at 1000 rpm. The beam intensity was monitored by measuring elastically scattered projectiles with a Si PIN photodiode (Hamamatsu S1223) mounted 1.42 m downstream of the target at 45° with respect to the beam axis. The beam energies at the middle of the target were calculated to be 121.2, 125.9, 130.6, 130.7, and 135.3 MeV using the stopping power model by Ziegler *et al.* [19] in the LISE++ program [20]. It is noted that the excitation functions calculated for the ^{248}Cm(^{23}Na,5n)^{266}Bh and ^{248}Cm(^{23}Na,4n)^{267}Bh reactions by the HIVAP code [21] exhibit the maximum cross sections of $\sigma = 60$ and 11 pb at 131 and 121 MeV, respectively (see Fig. 6). The typical beam intensity was 3 particle μA (pμA); 1 pμA corresponds to an impinging beam of 6.24×10^{12} particles/s. The evaporation residues (EVRs) of interest were separated in flight from the beam particles and the majority of the nuclear transfer products by GARIS and were guided to a focal plane of GARIS. GARIS was filled with helium gas at a pressure of 33 Pa and the magnetic rigidity $B\rho$ was 2.12 Tm. The efficiency for collecting ^{266}Bh at the focal plane of GARIS was estimated to be 15% based on our separate experiments with ^{255}No [22], ^{261}Rf^{a} [16], and ^{262}Db [12] produced in the ^{238}U(^{22}Ne,5n)^{255}No, ^{248}Cm(^{18}O,5n)^{261}Rf^{a}, and ^{248}Cm(^{19}F,5n)^{262}Db reactions, respectively.

At the focal plane of GARIS, a gas-jet chamber of 100-mm inner diameter and 20-mm depth was equipped. The EVRs separated with GARIS passed through a Mylar vacuum window foil of 0.7-μm thickness which was supported by a honeycomb-hole grid with 78.2% transparency. In the gas-jet chamber, the EVRs were thermalized in helium gas, attached to aerosol particles of potassium chloride, and were continuously transported through a Teflon capillary (2.0-mm inner diameter×10-m length) to the rotating wheel apparatus MANON for α and SF spectrometries [15–17], which was placed in a chemistry laboratory isolated with a 0.5-m concrete shield from an irradiation room. The flow rate of the helium gas was 5.0 l/min, and the inner pressure of the gas-jet chamber was 80 kPa. The gas-jet transport efficiency and the average transport time were estimated to be 50% and 3 s, respectively, based on our previous ^{248}Cm(^{18}O,5n)^{261}Rf^{a,b} experiments [16,17].

In MANON, the aerosol particles were deposited on a gold-coated (5 nm) Mylar foil of 0.5-μm thickness, 40 of which were set on the periphery of a rotating wheel. The wheel was stepped to position the foils between 15 pairs of Si PIN photodiodes (Hamamatsu S3204-09). The step intervals of MANON were set to 5.0, 8.5, and 15.0 s that resulted in measuring times of 0.3–75.0, 0.3–127.5, and 0.3–225.0 s for each sample with the 15 detectors; the detector dead time during the rotation of the wheel was 0.3 s for each step. Each Si PIN photodiode had an active area of 18×18 mm^2 and a 38% counting efficiency for the samples deposited on the Mylar foil. Each signal of the detector was divided into signals for α particles (1–20 MeV) and SF fragments (5–150 MeV). The α-energy resolution was about 50-keV full width at half maximum (FWHM) in the top detectors and about 100 keV in the bottom detectors; the latter was larger because of energy degradation in the Mylar foils. For daughter nuclides which recoiled out from the sample onto the top detector, the α-energy resolution would become larger than the above value in the top detectors due to the closer distance to the detector. All events were recorded in an event-by-event mode together with time information. During all irradiations, the wheels containing the Mylar foils were replaced every 12 h at the longest to prevent the buildup of the long-lived radioactivities.

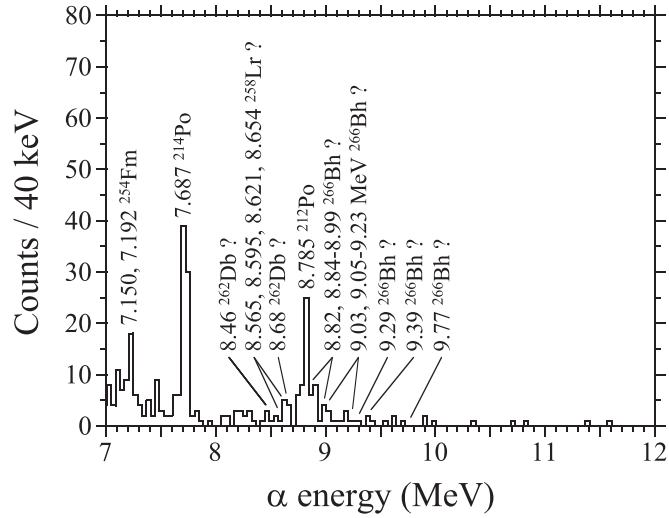

FIG. 2. Sum of α-particle spectra measured in the 15 top detectors of the rotating wheel apparatus MANON at the step interval of 8.5 s. The beam integral of 8.90×10^{18} was accumulated at 130.6 MeV. The $^{248}Cm_2O_3$ target with a thickness of 257 μg/cm^2 was used. The α groups reported for ^{266}Bh (E_α = 8.82, 8.84–8.99 MeV [11], 9.03 MeV [10], 9.05–9.23 MeV [7,11], 9.29 MeV [5], 9.39 MeV [9], and 9.77 MeV [8]), its α-decay daughter ^{262}Db (E_α = 8.46 and 8.68 MeV [12]) and granddaughter ^{258}Lr (E_α = 8.565, 8.595, 8.621, and 8.654 MeV [14]) are not very clear in the spectrum.

III. RESULTS

Figure 2 shows a typical example of α-particle spectrum measured in the 15 top detectors of MANON at the step interval of 8.5 s. The beam integral of 8.90×10^{18} was accumulated at 130.6 MeV where the excitation function for the ^{248}Cm(^{23}Na,5n)^{266}Bh reaction by the HIVAP code [21] exhibits the maximum cross section (see Fig. 6). In this measurement, six time-correlated α decays of ^{266}Bh were observed (chains 13–18 in Table IV). Due to the very small number of the events, however, α groups reported for ^{266}Bh (E_α = 8.82, 8.84–8.99 MeV [11], 9.03 MeV [10], 9.05–9.23 MeV [7,11], 9.29 MeV [5], 9.39 MeV [9], and 9.77 MeV [8]), its α-decay daughter ^{262}Db (E_α = 8.46 and 8.68 MeV [12]) and granddaughter ^{258}Lr (E_α = 8.565, 8.595, 8.621, and 8.654 MeV [14]) are not very clear in Fig. 2. After the GARIS separation, radioactivities due to α decays of multinucleon transfer reaction products from the Cm target as well as the Pb impurity in the target material or the target assembly were fairly suppressed compared with the previous ^{249}Bk + ^{22}Ne

TABLE IV. Correlated decay chains observed in this paper. Given are the number of the chain, the beam energy at which it was observed, the α energies of parent (E_1), daughter (E_2), and granddaughter (E_3), and the observed decay times of parent (τ_1), daughter (τ_2), and granddaughter (τ_3). τ_1 is defined as an elapsed time since the beginning of the measurement. Fission fragment energies are not corrected for pulse height defect and energy degradation in a Mylar foil for bottom detectors. The detector in which the event was observed is given in parentheses; "*T*" stands for top detectors, and "*B*" stands for bottom detectors. The classifications by groups $A-E$ in the two-dimensional plot of the correlated event pairs (Fig. 3) are also listed. In the last column, the decay assignments are given for each chain.

No.	Beam energy (MeV)	E_1 (MeV)	τ_1 (s)	E_2 (MeV)	τ_2 (s)	E_3 (MeV)	τ_3 (s)	Group	Decay assignment
1	125.9	9.01 (B2)	10.03	82/98 (T11/B11)	81.96			*B*	^{266}Bh → ^{262}Db →
2	125.9	8.75 (B2)	13.30	8.09 (T2)	246.09				Not assigned
3	125.9	9.25 (T1)	1.38	130/56 (T8/B8)	58.37			*B*	^{266}Bh → ^{262}Db →
4	125.9	8.96 (T3)	24.09	98/38 (T4/B4)	5.16			*B*	^{266}Bh → ^{262}Db →
5	130.6	9.40 (T4)	19.00	115/64 (T7/B7)	13.52			*B*	^{266}Bh → ^{262}Db →
6	130.6	8.80 (B6)	26.27	135/86 (T6/B6)	19.62			*B*	^{266}Bh → ^{262}Db →
7	130.6	9.05 (T12)	57.28	90/91 (T14/B14)	8.86			*B*	^{266}Bh → ^{262}Db →
8	130.6	8.66 (B1)	2.34	108/84 (T4/B4)	13.95			*D*	^{266}Bh → ^{262}Db → or ^{262}Db → ^{258}Lr(^{258}No) →
9	130.6	8.89 (B1)	5.17	8.49 (T1)	58.93	8.64 (T1)	8.38	*A*, *E*	^{266}Bh → ^{262}Db → ^{258}Lr →
10	130.6	8.84 (T1)	9.19	114/86 (T5/B5)	61.36			*B*	^{266}Bh → ^{262}Db →
11	130.6	8.67 (T13)	184.79	8.72 (T13)	7.77			*C*	^{262}Db → ^{258}Lr →
12	130.6	8.72 (T1)	7.40	8.74 (T5)	64.59			*C*	^{266}Bh → ^{262}Db / ^{258}Lr →
13	130.6	9.12 (T1)	0.92	8.70 (T2)	10.29	8.59 (T3)	7.05	*A*, *C*	^{266}Bh → ^{262}Db → ^{258}Lr →
14	130.6	8.85 (T1)	7.68	93/76 (T11/B11)	79.78			*B*	^{266}Bh → ^{262}Db →
15	130.6	8.86 (T2)	13.05	119/88 (T13/B13)	95.01			*B*	^{266}Bh → ^{262}Db →
16	130.6	8.98 (T2)	16.43	127/27 (T6/B6)	31.41			*B*	^{266}Bh → ^{262}Db →
17	130.6	8.71 (B5)	34.43	8.43 (T5)	44.26			*C*	^{266}Bh → ^{262}Db →
18	130.6	8.80 (B2)	13.65	8.62 (T2)	12.76			*A*	^{266}Bh → ^{262}Db / ^{258}Lr →
19	130.7	8.46 (T1)	0.47	8.50 (B1)	6.68			*E*	^{262}Db → ^{258}Lr →
20	130.7	8.62 (T1)	2.42	8.45 (T11)	89.48	8.63 (T11)	1.24	*C*, *E*	^{266}Bh → ^{262}Db → ^{258}Lr →
21	130.7	8.41 (B4)	30.63	8.67 (T4)	0.96			*E*	^{262}Db → ^{258}Lr →
22	130.7	8.97 (T2)	10.32	8.39 (B2)	2.72	8.62 (T2)	5.89	*A*, *E*	^{266}Bh → ^{262}Db → ^{258}Lr →
23	130.7	9.29 (B1)	4.10	69/102 (T1/B1)	186.72			*B*	^{266}Bh → ^{262}Db →
24	130.7	8.86 (T4)	33.65	133/89 (T9/B9)	40.50			*B*	^{266}Bh → ^{262}Db →
25	130.7	8.63 (B3)	23.98	8.61 (T4)	5.92			*C*	^{266}Bh → ^{262}Db / ^{258}Lr → or ^{262}Db → ^{258}Lr →
26	130.7	9.37 (T1)	5.97	8.46 (T11)	84.31			*A*	^{266}Bh → ^{262}Db →
27	130.7	9.17 (B2)	8.81	8.49 (T2)	19.75	8.61 (T3)	5.55	*A*, *E*	^{266}Bh → ^{262}Db → ^{258}Lr →
28	135.3	9.04 (B1)	0.33	8.63 (T1)	9.07	8.59 (T1)	4.64	*A*, *C*	^{266}Bh → ^{262}Db → ^{258}Lr →
29	135.3	8.43 (T5)	35.94	8.56 (T5)	1.33			*E*	^{262}Db → ^{258}Lr →
30	135.3	8.47 (B2)	16.51	8.32 (T3)	6.01			*E*	^{262}Db → ^{258}Lr →
31	135.3	8.25 (B8)	60.94	8.61 (T9)	7.53			*E*	^{262}Db → ^{258}Lr →
32	135.3	9.22 (T3)	21.17	8.46 (T5)	19.27	8.34 (B6)	4.00	*A*, *E*	^{266}Bh → ^{262}Db → ^{258}Lr →

and ^{243}Am + ^{26}Mg experiments (e.g., Fig. 2 of Ref. [5] and Fig. 2 of Ref. [10]). The prominent 7.687-MeV α line is due to ^{214}Po; ^{214}Po is a descendant of the natural radioisotope ^{222}Rn in the room, and its daughter nuclides stick to the detectors during a replacement of the Mylar foils. Similarly, the 8.785-MeV α line is ^{212}Po as a descendant of the natural radioisotope ^{220}Rn in the room.

For all events collected with MANON, we searched for time-correlated α-α event pairs in the α-energy ranges of $8.00\,\text{MeV} \leqslant E_\alpha \leqslant 10.00\,\text{MeV}$ and $8.00\,\text{MeV} \leqslant E_\alpha \leqslant 8.77\,\text{MeV}$ for the parent and daughter α events, respectively, based on the reported α energies of ^{266}Bh and ^{267}Bh and their daughters (see Fig. 1). We also searched for time-correlated α-SF event pairs in the parent α-energy range of $8.00\,\text{MeV} \leqslant E_\alpha \leqslant 10.00\,\text{MeV}$. The coincident events in the top and bottom detectors in the SF fragment energy range of $E_{\text{SF}} \geqslant 20\,\text{MeV}$ were assigned to SF. The time window for the search of the α-α and α-SF event pairs was set to 340 s which corresponds to 10 and 13 half-lives of the α- and SF-decay daughters ^{262}Db ($T_{1/2} = 33.8\,\text{s}$ [12]) and ^{263}Db ($T_{1/2} = 27\,\text{s}$ [13]) of ^{266}Bh and ^{267}Bh, respectively. As a result, a total of 31 α-α and 13 α-SF correlations were obtained. It is noted that 19 out of the 31 α-α compose seven triple-α correlations (α-α-α). The numbers of the α-α, α-α-α, and α-SF correlations are summarized in Table III. Random rates for those correlations were calculated by taking the observed number of all α events and multiplying by the probability of observing α or SF within the required time. The expected maximum numbers of the random correlations are listed in Table III, and they are less than 0.43, 0.01, and 0.06 for α-α, α-α-α, and α-SF, respectively. The details of all of the correlations are shown in Table IV where the beam energies, the α or SF fragment energies of parent (E_1), daughter (E_2), and granddaughter (E_3), the detectors in which the event was observed, and

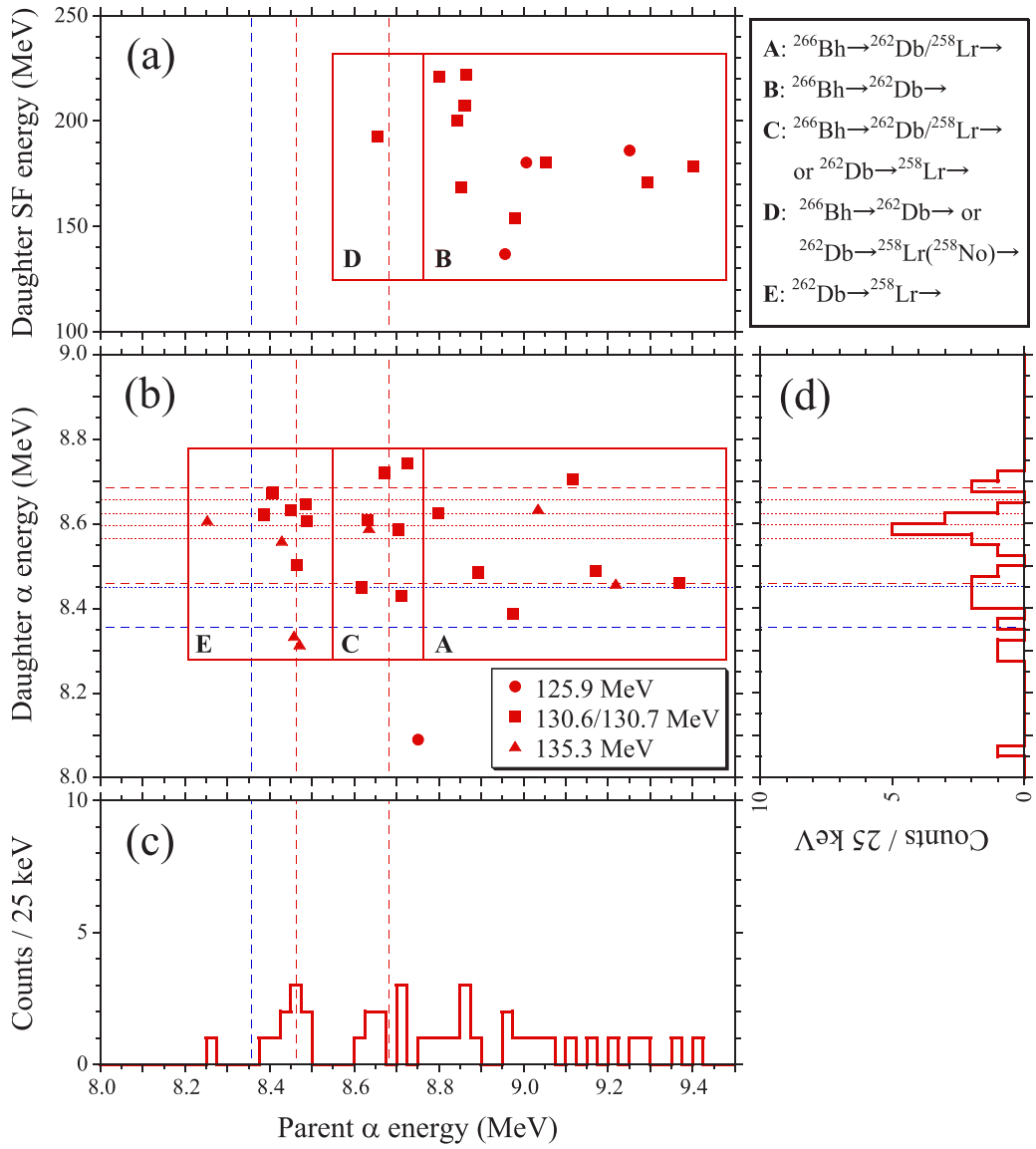

FIG. 3. Two-dimensional presentations of time-correlated events observed in the bombardment of ^{248}Cm with ^{23}Na ions: (a) α_1-SF (α_1: parent α) correlations and (b) α_1-α_2 (α_2: daughter α). The time-correlated events at the beam energies of 125.9, 130.6/130.7, 135.3 MeV are shown by closed circles, closed squares, and closed triangles, respectively. (c) α-particle spectrum of α_1. (d) α-particle spectrum of α_2. The expected α energies for ^{262}Db (E_α = 8.46 and 8.68 MeV [12]), ^{263}Db (E_α = 8.36 [13]), for their daughters ^{258}Lr (E_α = 8.565, 8.595, 8.621, and 8.654 MeV [14]), and ^{259}Lr (E_α = 8.45 MeV [14]) are indicated by dashed and dotted lines, respectively.

the observed decay times of parent (τ_1), daughter (τ_2), and granddaughter (τ_3) are listed. τ_1 is defined as an elapsed time since a beginning of the measurement.

Two-dimensional arrays of the time-correlated α-SF and α-α pairs are shown in Figs. 3(a) and 3(b), respectively. The pairs at the beam energies of 125.9, 130.6/130.7, 135.3 MeV are shown by closed circles, closed squares, and closed triangles, respectively. Figures 3(c) and 3(d) display the α spectra of parent and daughter, respectively. In the figures, the α energies reported for ^{262}Db (E_α = 8.46 and 8.68 MeV [12]) and ^{263}Db (E_α = 8.36 MeV [13]), their daughters ^{258}Lr (E_α = 8.565, 8.595, 8.621, and 8.654 MeV [14]) and ^{259}Lr (E_α = 8.45 MeV [14]) are indicated by dashed and dotted lines, respectively. Several α energies reported for ^{266}Bh (E_α = 8.82, 8.84–8.99 MeV [11], 9.03 MeV [10], 9.05–9.23 MeV [7,11], 9.29 MeV [5], 9.39 MeV [9], and 9.77 MeV [8]) and ^{267}Bh (E_α = 8.83 MeV [5]) are not indicated in the figures to make it easy to see the figures. The SF decay mode is known for ^{262}Db (b_{SF} = 52% [12]), ^{263}Db (b_{SF} = 55% [13]), and ^{259}Lr (b_{SF} = 23% [14]). The EC decay mode is known for ^{263}Db (b_{EC} = 3% [13]) and ^{258}Lr (b_{EC} = 2.6% [12]) and their EC decay daughters ^{263}Rf (b_{SF} = 100% [13]) and ^{258}No (b_{SF} = 100% [14]), respectively, decay by SF.

In this paper, no correlated α-SF and α-α pairs corresponding to the decay chain ^{263}Db → ^{259}Lr → were seen in Figs. 3(a) and 3(b), respectively, suggesting that few numbers of the ^{267}Bh atoms were produced in this experiment, and the predicted small cross sections for the ^{248}Cm(^{23}Na,4n)^{267}Bh

reaction at the studied energies would be reasonable (see Fig. 6).

Based on the reported α energies and decay patterns of ^{266}Bh and its daughters ^{262}Db and ^{258}Lr in Fig. 1, the correlated events can be classified into five groups *A*, *B*, *C*, *D*, and *E* in Figs. 3(a) and 3(b). These classifications are also indicated for each correlation in Table IV. The eight α-α pairs in group *A* can be assigned to the chain ^{266}Bh $\rightarrow$ ^{262}Db or ^{258}Lr $\rightarrow$. The daughter α energies agree with the reported data of ^{262}Db [12] and ^{258}Lr [14]. The 12 α-SF pairs in group *B* can be assigned to the chain ^{266}Bh $\rightarrow$ ^{262}Db $\rightarrow$; the possibility of assignment of the α-SF events to ^{266}Bh $\rightarrow$ (missing ^{262}Db $\rightarrow$ ^{258}Lr $\rightarrow$) ^{258}No $\rightarrow$ would be very small based on the small EC branch in ^{258}Lr ($b_{\rm EC} = 2.6\%$) [12]. The daughter half-life of $T_{1/2} = 32.3^{+9.2}_{-5.9}$ s (68% confidence interval (c.i.) [23]) calculated from the average decay time of the 20 pairs in groups *A* and *B* agrees with $T_{1/2} = 33.8^{+4.4}_{-3.5}$ s of ^{262}Db [12]. The $b_{\rm SF} = 60 \pm 11\%$ of the daughter nuclide is also consistent with $b_{\rm SF} = 52 \pm 4\%$ of ^{262}Db [12]. Thus, the parent α decays in groups *A* and *B* were reasonably assigned to ^{266}Bh.

The parent α energies of the pairs in groups *C*/*D* and *E* correspond to the 8.68- and 8.46-MeV α decays of ^{262}Db, respectively. All ten α-α pairs in group *E* were assigned to ^{262}Db $\rightarrow$ ^{258}Lr $\rightarrow$. Although the parent α energy of $E_\alpha = 8.25$ MeV (chain 31) and the daughter α energies of $E_\alpha = 8.32$ MeV (chain 30) and 8.34 MeV (chain 32) are more than 200 keV smaller than the lowest α energies of ^{262}Db ($E_\alpha = 8.46$ MeV [12]) and ^{258}Lr ($E_\alpha = 8.565$ MeV [14]), they are within the distributions of the measured α energies of ^{262}Db ($E_\alpha =$ 8.21–8.77 MeV) and ^{258}Lr ($E_\alpha =$ 8.26–8.73 MeV) with the same MANON setup in our previous ^{248}Cm(^{19}F,5*n*)^{262}Db experiment [12]. The daughter half-life of $T_{1/2} = 3.30^{+1.49}_{-0.78}$ s (68% c.i. [23]) deduced from the average decay time of the 10 α-α pairs in group *E* is consistent with $T_{1/2} = 3.54^{+0.46}_{-0.36}$ s of ^{258}Lr [12].

The one α-α-α pair in groups *C* and *E* (chain 20), i.e., α_1 ($E_\alpha = 8.62$ MeV; $\tau_1 = 2.42$ s) $\rightarrow$ α_2 ($E_\alpha = 8.45$ MeV; $\tau_2 =$ 89.48 s) $\rightarrow$ α_3 ($E_\alpha = 8.63$ MeV; $\tau_3 = 1.24$ s) $\rightarrow$ can be reasonably assigned to the chain ^{266}Bh $\rightarrow$ ^{262}Db $\rightarrow$ ^{258}Lr $\rightarrow$, although the α energy of $E_\alpha = 8.62$ MeV measured for ^{266}Bh with the top detector having the α-energy resolution of about 50-keV FWHM was smaller than those in Refs. [5,7–11] ($E_\alpha =$ 8.82–9.77 MeV). Since this low-α energy of ^{266}Bh ($E_\alpha = 8.62$ MeV) is close to $E_\alpha = 8.68$ MeV of its daughter ^{262}Db [12], the other six α-α pairs in group *C* and one α-SF pair in group *E* should be carefully judged. The latter α-α pairs (α_2-α_3) of the two α_1-α_2-α_3 (chains 13 and 28) in group *C* could be unambiguously assigned to ^{262}Db $\rightarrow$ ^{258}Lr $\rightarrow$. The α-α pair (chain 25) has two possible assignments to ^{266}Bh $\rightarrow$ ^{262}Db or ^{258}Lr $\rightarrow$ and ^{262}Db $\rightarrow$ ^{258}Lr $\rightarrow$ due to their indistinguishable α energies, whereas the α-α pair (chain 17) was assigned to ^{266}Bh $\rightarrow$ ^{262}Db $\rightarrow$; the daughter α energy of $E_\alpha = 8.43$ MeV measured with the top detector agrees with the characteristic $E_\alpha = 8.46$ MeV of ^{262}Db [12]. The α-α pair (chain 11) was assigned to ^{262}Db $\rightarrow$ ^{258}Lr $\rightarrow$ because the decay time of the parent ($\tau_1 = 184.79$ s) is too long for ^{266}Bh by considering its 10-s half-life (see Fig. 5). The α-α pair (chain 12) was assigned to ^{266}Bh $\rightarrow$ ^{262}Db or ^{258}Lr $\rightarrow$ not to ^{262}Db $\rightarrow$ ^{258}Lr $\rightarrow$ because the decay time of the daughter ($\tau_1 = 64.59$ s) is too long for ^{258}Lr with $T_{1/2} = 3.54^{+0.46}_{-0.36}$ s [12]. The α-SF pair (chain 8) in group *D* has two possible assignments to ^{266}Bh $\rightarrow$ ^{262}Db $\rightarrow$ and ^{262}Db $\rightarrow$ (missing ^{258}Lr $\rightarrow$) ^{258}No $\rightarrow$, although the possibility of the latter assignment is unlikely due to the very small EC branch in ^{258}Lr ($b_{\rm EC} = 2.6\%$) [12].

In Fig. 3(b), we observed one exceptional α-α pair: α_1 ($E_\alpha = 8.75$ MeV, $\tau_1 = 13.30$ s) $\rightarrow$ α_2 ($E_\alpha = 8.09$ MeV; $\tau_2 =$ 246.09 s) $\rightarrow$ (chain 2). This sequence is different from all known decay patterns of the nuclides of interest and would be of random origin. Thus, we assigned all the correlated α-SF and α-α pairs to ^{266}Bh $\rightarrow$ ^{262}Db $\rightarrow$ ^{258}Lr $\rightarrow$ except for chain 2 as indicated in the last column of Table IV. The half-lives of ^{262}Db and ^{258}Lr were determined to be $T_{1/2} = 33.7^{+9.3}_{-6.0}$ s (68% c.i. [23]) and $3.14^{+1.36}_{-0.76}$ s (68% c.i. [23]) from the average 21 and 12 decay times of ^{262}Db and ^{258}Lr, respectively, and they agree well with the reported $T_{1/2} = 33.8^{+4.4}_{-3.5}$ s [12] and $T_{1/2} = 3.54^{+0.46}_{-0.36}$ s [12], respectively.

IV. DISCUSSION

A. Decay properties of ^{266}Bh

As indicated in Table IV, a total of 23 α decays were assigned to ^{266}Bh in this paper. In Fig. 4(b), α spectrum of the 23 α decays of ^{266}Bh is shown. Compared in Figs. 4(c)–4(g) are the spectra of ^{266}Bh and/or ^{267}Bh reported in the ^{249}Bk(^{22}Ne,5;4*n*)^{266,267}Bh [5], ^{249}Bk(^{22}Ne,4*n*)^{267}Bh [6], ^{209}Bi(^{70}Zn,*n*)^{278}Nh $\rightarrow$ ^{266}Bh [7–9], ^{243}Am(^{26}Mg,3*n*)^{266}Bh [10], and ^{248}Cm(^{23}Na,5;4*n*)^{266,267}Bh [11] reactions, respectively. As shown in Fig. 4(b), the α-particle energies measured in this paper disperse widely in the range of $E_\alpha =$ 8.62–9.40 MeV, and α groups are not very clear in the spectrum. The reported α groups of $E_\alpha = 9.29$ MeV [5], 9.08 MeV [7], 9.39 MeV [9], 9.03 MeV [10], 8.82, 8.84–8.99, and 9.05–9.23 MeV [11] for ^{266}Bh are all within our α-energy range of $E_\alpha =$ 8.62–9.40 MeV except for $E_\alpha = 9.77$ MeV [8]. The widely dispersed α-decay energies of the odd-odd ^{266}Bh nucleus would be a natural feature due to the decays to lots of excited states in ^{262}Db; as an example, the α energies of the odd-odd ^{264}Bh nucleus disperse widely in the range of $E_\alpha =$ 8.87–9.85 MeV [24].

In Fig. 4(a), the decay times of the α decays of ^{266}Bh measured in this paper are shown by closed squares as a function of the α energy together with those of ^{266}Bh and ^{267}Bh reported in Refs. [5–10]. No decay times were measured in Ref. [11] as described in the Introduction. The decay times measured in this paper at $E_\alpha <$ ~9.1 MeV seem to be longer than those at $E_\alpha >$ ~9.1 MeV, suggesting that isomeric states would exist in ^{266}Bh. The half-lives deduced from the average decay times of the 16 α decays at $E_\alpha < 9.10$ MeV and the 7 α decays at $E_\alpha \geqslant 9.10$ MeV are $T_{1/2} = 11.8^{+3.9}_{-2.3}$ and $6.1^{+3.6}_{-1.6}$ s (68% c.i. [23]), respectively, and they are consistent with each other within the error. A high-resolution α-particle spectrometry with a large number of decay events would be desired to confirm the existence of the isomeric states in

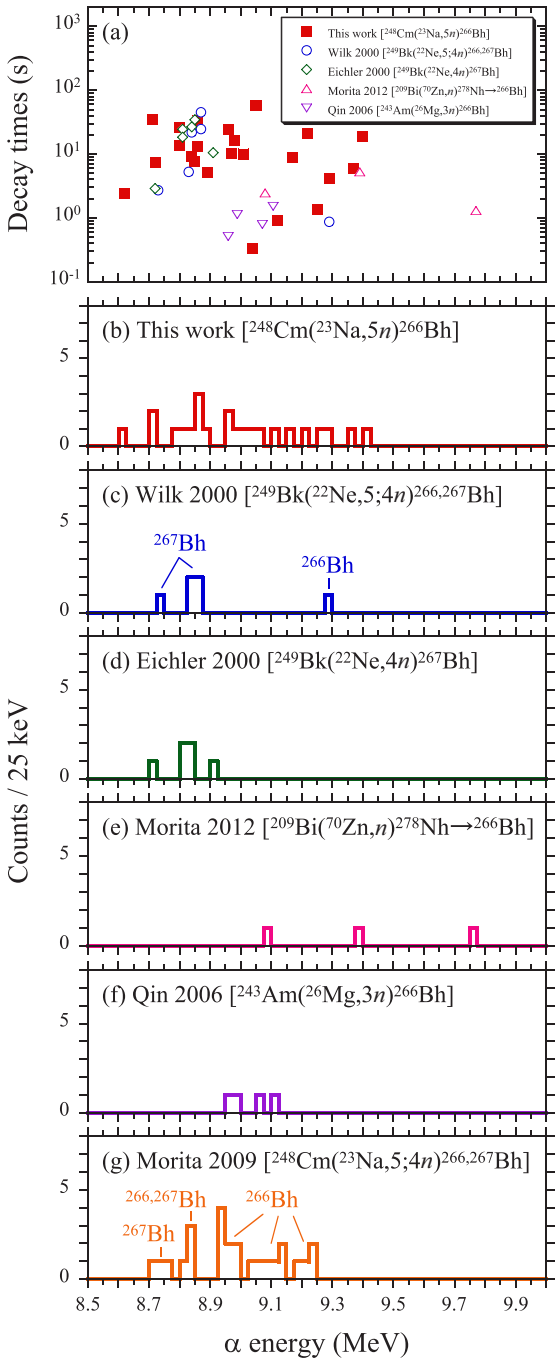

FIG. 4. (a) Decay times of the α decays of ^{266}Bh observed in this paper as a function of the α-particle energy (closed squares). The literature data on ^{266}Bh and ^{267}Bh (Wilk *et al.* [5], Eichler *et al.* [6], Morita and co-workers [7–9], and Qin *et al.* [10]) are compared. (b) α-particle spectrum of ^{266}Bh produced in the ^{248}Cm(^{23}Na,5n)^{266}Bh reaction in this paper. (c) α spectrum of ^{266}Bh and ^{267}Bh produced in the ^{249}Bk(^{22}Ne,5;4n)^{266,267}Bh reactions (Wilk *et al.* [5]). (d) α spectrum of ^{267}Bh produced in the ^{249}Bk(^{22}Ne,4n)^{267}Bh reaction (Eichler *et al.* [6]). (e) α spectrum of ^{266}Bh on the α-decay chain of ^{278}Nh produced in the ^{209}Bi(^{70}Zn,n)^{278}Nh reaction (Morita and co-workers [7–9]). (f) α spectrum of ^{266}Bh produced in the ^{243}Am(^{26}Mg,3n)^{266}Bh reaction (Qin 2006: [10]). (g) α spectrum of ^{266}Bh and ^{267}Bh produced in the ^{248}Cm(^{23}Na,5;4n)^{266,267}Bh reactions (Morita *et al.* [11]).

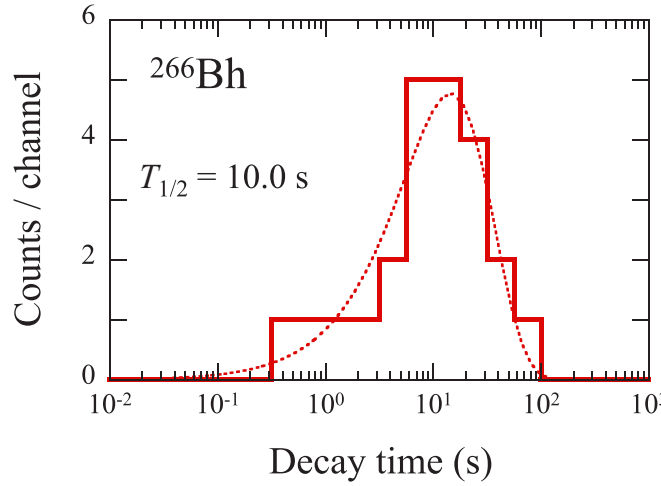

FIG. 5. Spectrum of decay times of ^{266}Bh. The counts in a radioactive decay are shown on a logarithmic time scale with a logarithmically increasing channel width. The best fit is shown by the dotted curve.

^{266}Bh. The decay time distribution for the α decays observed in this paper is shown in Fig. 5. The half-life deduced from the average decay time is $T_{1/2} = 10.0^{+2.6}_{-1.7}$ s (68% c.i. [23]), and this value is an order of magnitude longer than the literature data of $T_{1/2} = \sim$1 s [5] and $T_{1/2} = 0.66^{+0.59}_{-0.26}$ s [11], and five times longer than $T_{1/2} = 2.1^{+2.9}_{-0.8}$ s in Refs. [7–9].

As mentioned in the Introduction, a total of 15 α decays of ^{267}Bh with $E_\alpha = 8.83$ MeV [5], 8.72–8.91 MeV [6] and 8.71–8.84 MeV [11] were reported based on the correlated α-decay chains to its daughter ^{263}Db and granddaughter ^{259}Lr. However, these α decays of ^{267}Bh cannot be clearly distinguished from those of ^{266}Bh because of their indistinguishable α energies and decay times as well as the similar decay properties of their daughters. Wilk *et al.* [5] reported the three and two α-α correlations of ^{267}Bh produced in the ^{249}Bk(^{22}Ne,4n)^{267}Bh reaction at the beam energies of 117 and 123 MeV, respectively. Due to relatively large α radioactivities of byproducts, one of the five pairs was estimated to be a random correlation of unrelated α decays. The daughter α energies of $E_\alpha = 8.36$–8.47 MeV in the five correlations are consistent with not only $E_\alpha = 8.36$ MeV of ^{263}Db and $E_\alpha = 8.45$ MeV of ^{269}Lr, but also $E_\alpha = 8.46$ MeV of ^{262}Db, the daughter of ^{266}Bh within the resolution of the PIPS detector used in Ref. [5] (FWHM = 0.04–0.10 MeV). Eichler *et al.* [6] reported the six α decays of ^{267}Bh (one random) in the ^{249}Bk(^{22}Ne,4n)^{267}Bh reaction at 119 MeV. The three α-SF pairs assigned to the chain ^{267}Bh $\rightarrow$ ^{263}Db / ^{259}Lr $\rightarrow$ cannot be distinguished from ^{266}Bh $\rightarrow$ ^{262}Db $\rightarrow$ due to the similar SF properties between ^{263}Db / ^{259}Lr and ^{262}Db. Although one α-α-α pair was reasonably assigned to ^{267}Bh $\rightarrow$ ^{263}Db $\rightarrow$ ^{259}Lr $\rightarrow$, the two α-α pairs of ^{267}Bh $\rightarrow$ ^{263}Db / ^{259}Lr $\rightarrow$ are in question due to the close α energies between ^{263}Db / ^{259}Lr and ^{262}Db as described above. In addition, Wilk *et al.* [5] produced ^{266}Bh in the ^{249}Bk(^{22}Ne,5n)^{266}Bh reaction at 123 MeV with the comparable cross section of $\sigma = 25$–250 to $\sigma = 96^{+55}_{-25}$ pb for the ^{249}Bk(^{22}Ne,4n)^{267}Bh reaction [5]. It is

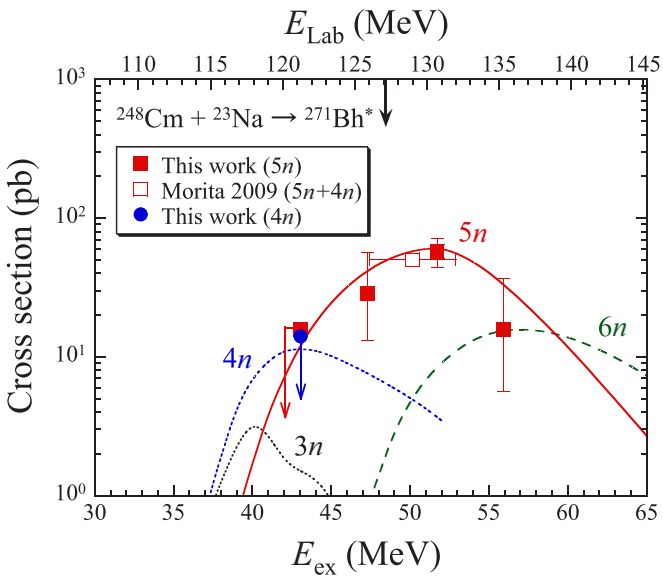

FIG. 6. Cross sections for the ^{248}Cm(^{23}Na,5n)^{266}Bh (closed square) and ^{248}Cm(^{23}Na,4n)^{267}Bh (closed circle) reactions as a function of the excitation energy $E_{\rm ex}$ and the laboratory-frame energy $E_{\rm Lab}$ (scale at the top). Curves are the HIVAP calculations [21] for the ^{248}Cm(^{23}Na,xn)$^{271-x}$Bh reactions (x = 3–6) according to the calculational method described in Refs. [25,26]. The energy-averaged and inclusive cross section for the 5n and 4n cannels at 126–132 MeV by Morita *et al.* [11] is compared by an open square. Error bars on the cross-sectional data correspond to 68% confidence intervals. The symbols with arrows denote upper limits. The location of the Bass barrier [29] (Bass interaction barrier) is indicated by the bold arrow on the upper horizontal axis.

noted here that the cross sections predicted by the HIVAP code [21] for the ^{249}Bk(^{22}Ne,4n)^{267}Bh reaction are smaller than those for the ^{249}Bk(^{22}Ne,5n)^{266}Bh reaction at the beam energies studied in Refs. [5,6] (see Fig. 7). Thus, the possibility of misassignment of the ^{266}Bh decays to ^{267}Bh cannot be excluded in Refs. [5,6]. The shapes of the α spectra in Figs. 4(c) and 4(d) are similar to that of ^{266}Bh in Fig. 4(b) in this paper, although the observed numbers of the events are small.

In the ^{248}Cm(^{23}Na,xn)$^{271-x}$Bh reactions at 126, 130, and 132 MeV, Morita *et al.* [11] assigned the four α-SF pairs to ^{267}Bh → ^{263}Db →, although they claimed that the possible assignment to ^{266}Bh → ^{262}Db → could not be excluded. Only one α-α-SF decay chain of ^{267}Bh (E_α = 8.84 MeV) → ^{263}Db (E_α = 8.42 MeV; τ = 11.95 s) → ^{259}Lr ($E_{\rm SF}$ = 169.5 MeV; τ = 27.22 s) → was observed at the beam energy of 132 MeV where the cross section for ^{266}Bh is expected to be an order of magnitude larger than that for ^{267}Bh (see Fig. 6). In our previous study [12], the EC decay mode was observed in ^{258}Lr and its EC decay daughter ^{258}No ($T_{1/2}$ = ∼1.2 ms) immediately decays by SF. Thus, the possibility of misassignment of the chain ^{266}Bh → ^{262}Db → ^{258}Lr → to ^{267}Bh → ^{263}Db → ^{259}Lr → in Ref. [11] cannot be excluded. The α spectrum of ^{266}Bh and ^{267}Bh produced in the ^{248}Cm(^{23}Na,5;4n)^{266,267}Bh reactions [11] [Fig. 4(g)] is compatible with that of ^{266}Bh in this paper in Fig. 4(b).

B. Cross section

Figure 6 shows the excitation functions predicted by the statistical model code HIVAP [21] for the ^{248}Cm(^{23}Na,xn)$^{271-x}$Bh reactions (x = 3–6). The details of our calculational method, such as the input parameters of the code, are described in Refs. [25,26]. In the entrance channel, an orientation of the deformed target nucleus was taken into account to calculate the Coulomb barrier and capture cross sections. Due to the light projectile and high mass asymmetry of the entrance channel, the fusion cross sections are almost equal to the capture cross sections. Our calculations successfully reproduced the excitation functions measured for the asymmetric reactions, such as ^{238}U(^{16}O,xn)$^{254-x}$Fm (x = 4–6) [25], ^{248}Cm(^{18}O,xn)$^{266-x}$Rf (x = 4–6) [27], ^{248}Cm(^{19}F,5n)^{262}Db [12], ^{248}Cm(^{22}Ne,5n)^{265}Sg [18], and ^{248}Cm(^{26}Mg,xn)$^{274-x}$Hs (x = 3–5) [28].

In this paper, we evaluated the cross sections for the ^{248}Cm(^{23}Na,5n)^{266}Bh and ^{248}Cm(^{23}Na,4n)^{267}Bh reactions in the following way. The 23 decay events of ^{266}Bh except for the alternative (chains 8 and 25 in Table IV) were used to evaluate the cross sections. The decay corrections due to the limited measuring time of MANON as well as the gas-jet transport time were conducted using the half-lives of $T_{1/2}$ = 10.0 s obtained for ^{266}Bh in this paper and $T_{1/2}$ = 17 s for ^{267}Bh in Ref. [5]. The α and SF decay branches of ^{266}Bh and ^{267}Bh and their daughters were shown in Fig. 1. The transport efficiencies of GARIS were assumed to be identical for the Bh isotopes irrespectively of the beam energies and the reaction channels. The cross sections for the ^{248}Cm(^{23}Na,5n)^{266}Bh reaction were determined to be $\sigma = 29^{+28}_{-16}$, 57 ± 14, and16^{+21}_{-10} pb (68% c.i. [23]) at 125.9, 130.6, and 135.3 MeV, respectively; the cross section at 130.7 MeV was merged with that at 130.6 MeV because the energy difference of 0.1 MeV is small enough as compared to the energy loss in the ^{248}Cm$_2$O$_3$ target (0.7 MeV [19,20]). At 121.2 MeV, the upper-limit cross section of $\sigma \leqslant 16$ pb (68% c.i. [23]) was evaluated. For the ^{248}Cm(^{23}Na,4n)^{267}Bh reaction, the upper limit of $\sigma \leqslant 14$ pb (68% c.i. [23]) was determined at 121.2 MeV. These cross sections are shown in Fig. 6 by closed squares and a closed circle for the ^{248}Cm(^{23}Na,5n)^{266}Bh and ^{248}Cm(^{23}Na,4n)^{267}Bh reactions, respectively. In the figure, the energy-averaged and inclusive cross section of σ = 50 pb at 126–132 MeV, reported by Morita *et al.* [11] for the ^{248}Cm(^{23}Na,5n) ^{266}Bh and ^{248}Cm(^{23}Na,4n)^{267}Bh reactions at 126–132 MeV, is also shown by an open square. The inclusive cross sections of ^{266}Bh and ^{267}Bh are consistent with our results on ^{266}Bh within the error. The HIVAP code reproduces well the experimental cross sections for the ^{248}Cm(^{23}Na,5n)^{266}Bh reaction as well as the upper limit for the ^{248}Cm(^{23}Na,4n)^{267}Bh reaction at 121.2 MeV. The location of the Bass barrier [29] (Bass interaction barrier) is indicated in Fig. 6 by the bold arrow on the upper horizontal axis. The excitation function for the ^{248}Cm(^{23}Na,5n)^{266}Bh reaction shows the maximum around the Bass fusion barrier [29]. The cross sections at the subbarrier energies arise from the capture cross sections due to the lower Coulomb barrier when the projectile collides on the polar sides of the deformed target nucleus [30,31].

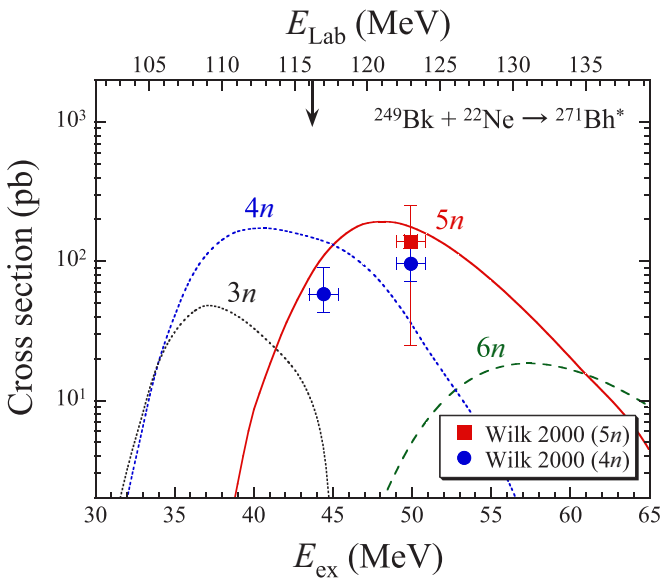

FIG. 7. Cross sections reported by Wilk *et al.* [5] for the ^{249}Bk(^{22}Ne,5*n*)^{266}Bh (closed square) and ^{249}Bk(^{22}Ne,4*n*)^{267}Bh (closed circle) reactions as a function of the excitation energy $E_{\rm ex}$ and the laboratory-frame energy $E_{\rm Lab}$ (scale at the top). Curves are the HIVAP calculations [21] for the ^{249}Bk(^{22}Ne,*xn*)$^{271-x}$Bh reactions (x = 3–6) according to the calculational method described in [25,26]. See the caption for Fig. 6 for others.

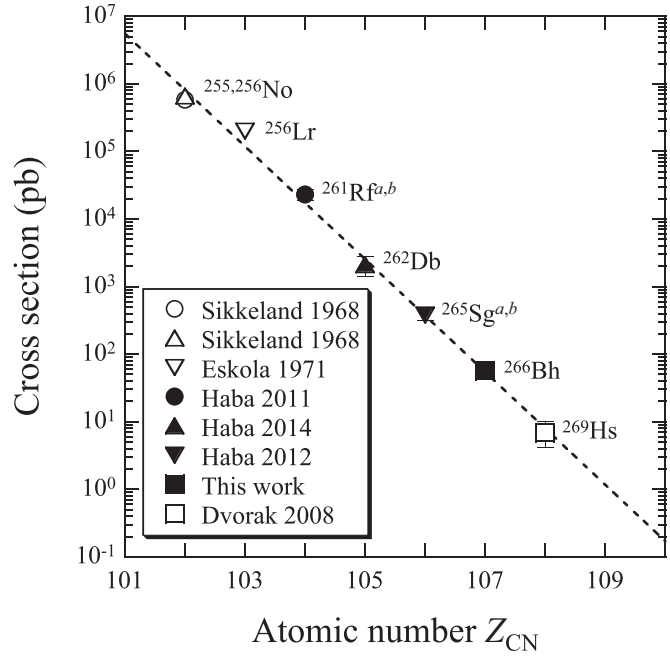

FIG. 8. Maximal cross sections of the 5*n* evaporation channel in the complete fusion reactions of ^{248}Cm target with different projectiles as a function of the compound nucleus atomic number $Z_{\rm CN}$. The present cross section for the ^{248}Cm(^{23}Na,5*n*)^{266}Bh reaction (closed square) is compared with the literature data for ^{248}Cm(^{12}C,5*n*)^{255}No (open circle, Sikkeland *et al.* [32]), ^{248}Cm(^{13}C,5*n*)^{256}No (open triangle, Sikkeland *et al.* [32]), ^{248}Cm(^{15}N,5*n*)^{256}Lr (open inverted triangle, Eskola *et al.* [33]), ^{248}Cm(^{18}O,5*n*)^{261}Rf^{a,b} (closed circle, Haba *et al.* [17]), ^{248}Cm(^{19}F,5*n*)^{262}Db (closed triangle, Haba *et al.* [12]), ^{248}Cm(^{22}Ne,5*n*)^{265}Sg^{a,b} (closed inverted triangle, Haba *et al.* [18]), and ^{248}Cm(^{26}Mg,5*n*)^{269}Hs (open square, Dvorak *et al.* [28]). The dashed line is an exponential fit to the data points.

It is interesting to compare the excitation functions for the ^{248}Cm + ^{23}Na and ^{249}Bk + ^{22}Ne reactions, which form the same compound nucleus of ^{271}Bh*. By using the same input parameters on the HIVAP code, the excitation functions for the ^{249}Bk(^{22}Ne,*xn*)$^{271-x}$Bh (x = 3–6) reactions were calculated as shown in Fig. 7. Due to large differences in the Bass barrier and Q values between the ^{248}Cm + ^{23}Na and the ^{249}Bk + ^{22}Ne reactions, a relatively larger contribution of the 4*n* channel was predicted in the ^{249}Bk + ^{22}Ne reaction. In Fig. 7, the cross sections reported by Wilk *et al.* [5] for the ^{249}Bk(^{22}Ne,5*n*)^{266}Bh reaction at 123 MeV and for the ^{249}Bk(^{22}Ne,4*n*)^{267}Bh reaction at 117 and 123 MeV are compared. The HIVAP code reproduces the 5*n* cross section at 123 MeV within the large error, whereas the code underestimates the 4*n* cross section at 123 MeV and conversely overestimates at 117 MeV. As discussed above, if the decay events previously assigned to ^{267}Bh in Ref. [5] attribute to ^{266}Bh, the sum cross sections can be reasonably reproduced by the HIVAP code. More detailed studies, however, would be desirable to gain further insight into the production and decay properties of ^{267}Bh in the ^{249}Bk(^{22}Ne,4*n*)^{267}Bh reaction at the lower excitation energies ($E_{\rm ex}$ < 40 MeV), where the 5*n* channel cannot be opened and unambiguous identification of ^{267}Bh would be possible.

In Fig. 8, the maximum cross section obtained for the ^{248}Cm(^{23}Na,5*n*)^{266}Bh reaction in this paper is shown as a function of the atomic number of compound nucleus ($Z_{\rm CN}$) together with those measured for ^{248}Cm(^{18}O,5*n*)^{261}Rf^{a,b} [17], ^{248}Cm(^{19}F,5*n*)^{262}Db [12], and ^{248}Cm(^{22}Ne,5*n*)^{265}Sg^{a,b} [18] at RIKEN. In Fig. 8, the literature data for ^{248}Cm(^{12}C,5*n*)^{255}No [32], ^{248}Cm(^{13}C,5*n*)^{256}No [32], ^{248}Cm(^{15}N,5*n*)^{256}Lr [33], and ^{248}Cm(^{26}Mg,5*n*)^{269}Hs [28] are also included. As can be seen in Fig. 8, the cross section for the 5*n* evaporation channel in the complete fusion reactions of ^{248}Cm with different projectiles exponentially decreases with $Z_{\rm CN}$. The cross section for element 109 ^{270}Mt, which was first observed as the granddaughter of ^{278}Nh produced in the cold fusion reaction of ^{209}Bi(^{70}Zn,*n*)^{278}Nh [7–9], is predicted to be about 1 pb *via* the ^{248}Cm(^{27}Al,5*n*)^{270}Mt reaction. The systematics is preserved in so far as the fusion probability after penetrating the Coulomb barrier does not drop significantly also in the ^{27}Al-induced reaction. This is verified from the reaction study using the ^{30}Si beam in the ^{238}U + ^{30}Si reaction [31] where the fusion hindrance is not evident around the Bass barrier from the measured evaporation-residue cross section of ^{263}Sg (5*n*).

V. CONCLUSIONS

The decay properties of ^{266}Bh produced in the ^{248}Cm(^{23}Na,5*n*)^{266}Bh reaction were investigated with the rotating wheel apparatus MANON under low background conditions attained by a gas-jet transport system coupled

to GARIS. Based on the genetically correlated α-α(-α) and α-SF decay chains of ^{266}Bh and its known daughter nuclide ^{262}Db and granddaughter nuclide ^{258}Lr, the α decays with $E_\alpha = 8.62$–9.40 MeV were assigned to ^{266}Bh. The half-life of $T_{1/2} = 10.0^{+2.6}_{-1.7}$ s obtained for ^{266}Bh is an order of magnitude longer than the literature data. This half-life is long enough to study chemical properties of Bh in future using the ^{248}Cm(^{23}Na,5n)^{266}Bh reaction. A question of the misassignment of the ^{266}Bh decays to ^{267}Bh in the previous studies was raised. The excitation function for the ^{248}Cm(^{23}Na,5n)^{266}Bh reaction was measured for the first time, and it indicates the maximum of $\sigma = 57 \pm 14$ pb at 130.6 MeV. The excitation function was reproduced by the statistical model code HIVAP. The upper-limit cross sections of $\sigma \leqslant 14$ pb was also derived for the ^{248}Cm(^{23}Na,4n)^{267}Bh reaction at 121.2 MeV.

ACKNOWLEDGMENTS

This work was performed at the RI Beam Factory operated by RIKEN Nishina Center and CNS, University of Tokyo. The authors express their gratitude to the crew of the RIKEN linear accelerator for their invaluable assistance in the course of the experiment. This research was partially supported by the Ministry of Education, Culture, Sports, Science, and Technology, Japan, Grant-in-Aids No. 19002005, No. 26286082, and No. 17H01081, and by the National Natural Science Foundation, China, Grants No. 11675227 and No. 11079006.

[1] A. Sobiczewski and K. Pomorski, Prog. Part. Nucl. Phys. **58**, 292 (2007).
[2] J. H. Hamilton, S. Hofmann, and Y. T. Oganessian, Annu. Rev. Nucl. Part. Sci. **63**, 383 (2013).
[3] Y. T. Oganessian and V. K. Utyonkov, Nucl. Phys. A **944**, 62 (2015).
[4] S. Hofmann, J. Phys. G: Nucl. Part. Phys. **42**, 114001 (2015).
[5] P. A. Wilk, K. E. Gregorich, A. Türler, C. A. Laue, R. Eichler, V. Ninov, J. L. Adams, U. W. Kirbach, M. R. Lane, D. M. Lee, J. B. Patin, D. A. Shaughnessy, D. A. Strellis, H. Nitsche, and D. C. Hoffman, Phys. Rev. Lett. **85**, 2697 (2000).
[6] R. Eichler, W. Brüchle, R. Dressler, C. E. Düllmann, B. Eichler, H. W. Gäggeler, K. E. Gregorich, D. C. Hoffman, S. Hübener, D. T. Jost, U. W. Kirbach, C. A. Laue, V. M. Lavanchy, H. Nitsche, J. B. Patin, D. Piguet, M. Schädel, D. A. Shaughnessy, D. A. Strellis, S. Taut, L. Tobler, Y. S. Tsyganov, A. Türler, A. Vahle, P. A. WiIk, and A. B. Yakushev, Nature (London) **407**, 63 (2000).
[7] K. Morita, K. Morimoto, D. Kaji, T. Akiyama, S. Goto, H. Haba, E. Ideguchi, R. Kanungo, K. Katori, H. Koura, H. Kudo, T. Ohnishi, A. Ozawa, T. Suda, K. Sueki, H. Xu, T. Yamaguchi, A. Yoneda, A. Yoshida, and Y. Zhao, J. Phys. Soc. Jpn. **73**, 2593 (2004).
[8] K. Morita, K. Morimoto, D. Kaji, T. Akiyama, S. Goto, H. Haba, E. Ideguchi, K. Katori, H. Koura, H. Kikunaga, H. Kudo, T. Ohnishi, A. Ozawa, N. Sato, T. Suda, K. Sueki, F. Tokanai, T. Yamaguchi, A. Yoneda, and A. Yoshida, J. Phys. Soc. Jpn. **76**, 045001 (2007).
[9] K. Morita, K. Morimoto, D. Kaji, H. Haba, K. Ozeki, Y. Kudou, T. Sumita, Y. Wakabayashi, A. Yoneda, K. Tanaka, S. Yamaki, R. Sakai, T. Akiyama, S. Goto, H. Hasebe, M. Huang, T. Huang, E. Ideguchi, Y. Kasamatsu, K. Katori, Y. Kariya, H. Kikunaga, H. Koura, H. Kudo, A. Mashiko, K. Mayama, S. Mitsuoka, T. Moriya, M. Murakami, H. Murayama, S. Namai, A. Ozawa, N. Sato, K. Sueki, M. Takeyama, F. Tokanai, T. Yamaguchi, and A. Yoshida, J. Phys. Soc. Jpn. **81**, 103201 (2012).
[10] Z. Qin, X.-L. Wu, H.-J. Ding, W.-S. Wu, W.-X. Huang, X.-G. Lei, Y.-B. Xu, X.-H. Yuan, B. Guo, W.-F. Yang, Z.-G. Gan, H.-M. Fan, J.-S. Guo, H.-S. Xu, and G.-Q. Xiao, Nucl. Phys. Rev. **23**, 400 (2006).
[11] K. Morita, K. Morimoto, D. Kaji, H. Haba, K. Ozeki, Y. Kudou, N. Sato, T. Sumita, A. Yoneda, T. Ichikawa, Y. Fujimori, S. Goto, E. Ideguchi, Y. Kasamatsu, K. Katori, Y. Komori, H. Koura, H. Kudo, K. Ooe, A. Ozawa, F. Tokanai, K. Tsukada, T. Yamaguchi, and A. Yoshida, J. Phys. Soc. Jpn. **78**, 064201 (2009).
[12] H. Haba, M. Huang, D. Kaji, J. Kanaya, Y. Kudou, K. Morimoto, K. Morita, M. Murakami, K. Ozeki, R. Sakai, T. Sumita, Y. Wakabayashi, A. Yoneda, Y. Kasamatsu, Y. Kikutani, Y. Komori, K. Nakamura, A. Shinohara, H. Kikunaga, H. Kudo, K. Nishio, A. Toyoshima, and K. Tsukada, Phys. Rev. C **89**, 024618 (2014).
[13] J. V. Kratz, A. Nähler, U. Rieth, A. Kronenberg, B. Kuczewski, E. Strub, W. Brüchle, M. Schädel, B. Schausten, A. Türler, H. W. Gäggeler, D. T. Jost, K. E. Gregorich, H. Nitsche, C. Laue, R. Sudowe, and P. A. Wilk, Radiochim. Acta **91**, 59 (2003).
[14] R. B. Firestone and V. S. Shirley, *Table of Isotopes*, 8th ed. (Wiley, New York, 1996).
[15] H. Haba, D. Kaji, H. Kikunaga, T. Akiyama, N. Sato, K. Morimoto, A. Yoneda, K. Morita, T. Takabe, and A. Shinohara, J. Nucl. Radiochem. Sci. **8**, 55 (2007).
[16] H. Haba, D. Kaji, Y. Komori, Y. Kudou, K. Morimoto, K. Morita, K. Ooe, K. Ozeki, N. Sato, A. Shinohara, and A. Yoneda, Chem. Lett. **38**, 426 (2009).
[17] H. Haba, D. Kaji, H. Kikunaga, Y. Kudou, K. Morimoto, K. Morita, K. Ozeki, T. Sumita, A. Yoneda, Y. Kasamatsu, Y. Komori, K. Ooe, and A. Shinohara, Phys. Rev. C **83**, 034602 (2011).
[18] H. Haba, D. Kaji, Y. Kudou, K. Morimoto, K. Morita, K. Ozeki, R. Sakai, T. Sumita, A. Yoneda, Y. Kasamatsu, Y. Komori, A. Shinohara, H. Kikunaga, H. Kudo, K. Nishio, K. Ooe, N. Sato, and K. Tsukada, Phys. Rev. C **85**, 024611 (2012).
[19] J. F. Ziegler, J. P. Biersack, and U. Littmark, *The Stopping and Range of Ions in Solid* (Pergamon Press, New York, 1985).
[20] O. B. Tarasov and D. Bazin, Nucl. Instrum. Methods Phys. Res. Sect. B **266**, 4657 (2008).
[21] W. Reisdorf and M. Schädel, Z. Phys. A **343**, 47 (1992).
[22] H. Haba, H. Kikunaga, D. Kaji, T. Akiyama, K. Morimoto, K. Morita, T. Nanri, K. Ooe, N. Sato, A. Shinohara, D. Suzuki, T. Takabe, I. Yamazaki, A. Yokoyama, and A. Yoneda, J. Nucl. Radiochem. Sci. **9**, 27 (2008).
[23] K.-H. Schmidt, C.-C. Sahm, K. Pielenz, and H.-G. Clerc, Z. Phys. A: At. Nucl. **316**, 19 (1984).
[24] K. Morita, K. Morimoto, D. Kaji, H. Haba, E. Ideguchi, J. C. Peter, R. Kanungo, K. Katori, H. Koura, H. Kudo, T. Ohnishi, A. Ozawa, T. Suda, K. Sueki, I. Tanihata, H. Xu, A. V. Yeremin, A. Yoneda, A. Yoshida, Y.-L. Zhao, T.

Zheng, S. Goto, and F. Tokanai, J. Phys. Soc. Jpn. **73**, 1738 (2004).

[25] K. Nishio, H. Ikezoe, Y. Nagame, M. Asai, K. Tsukada, S. Mitsuoka, K. Tsuruta, K. Satou, C. J. Lin, and T. Ohsawa, Phys. Rev. Lett. **93**, 162701 (2004).

[26] K. Nishio, S. Hofmann, F. P. Heßberger, D. Ackermann, S. Antalic, Y. Aritomo, V. F. Comas, C. E. Düllmann, A. Gorshkov, R. Graeger, K. Hagino, S. Heinz, J. A. Heredia, K. Hirose, H. Ikezoe, J. Khuyagbaatar, B. Kindler, I. Kojouharov, B. Lommel, R. Mann, S. Mitsuoka, Y. Nagame, I. Nishinaka, T. Ohtsuki, A. G. Popeko, S. Saro, M. Schädel, A. Türler, Y. Watanabe, A. Yakushev, and A. V. Yeremin, Phys. Rev. C **82**, 024611 (2010).

[27] M. Murakami, S. Goto, H. Murayama, T. Kojima, H. Kudo, D. Kaji, K. Morimoto, H. Haba, Y. Kudou, T. Sumita, R. Sakai, A. Yoneda, K. Morita, Y. Kasamatsu, H. Kikunaga, and T. K. Sato, Phys. Rev. C **88**, 024618 (2013).

[28] J. Dvorak, W. Brüchle, M. Chelnokov, C. E. Düllmann, Z. Dvorakova, K. Eberhardt, E. Jäger, R. Krücken, A. Kuznetsov, Y. Nagame, F. Nebel, K. Nishio, R. Perego, Z. Qin, M. Schädel, B. Schausten, E. Schimpf, R. Schuber, A. Semchenkov, P. Thörle, A. Türler, M. Wegrzecki, B. Wierczinski, A. Yakushev, and A. Yeremin, Phys. Rev. Lett. **100**, 132503 (2008).

[29] R. Bass, Nucl. Phys. **A231**, 45 (1974).

[30] K. Nishio, S. Hofmann, F. P. Heßberger, D. Ackermann, S. Antalic, V. F. Comas, Z. Gan, S. Heinz, J. A. Heredia, H. Ikezoe, J. Khuyagbaatar, B. Kindler, I. Kojouharov, P. Kuusiniemi, B. Lommel, R. Mann, M. Mazzocco, S. Mitsuoka, Y. Nagame, T. Ohtsuki, A. G. Popeko, S. Saro, H. J. Schött, B. Sulignano, A. Svirikhin, K. Tsukada, K. Tsuruta, and A. V. Yeremin, Eur. Phys. J. A **29**, 281 (2006).

[31] K. Nishio, H. Ikezoe, I. Nishinaka, S. Mitsuoka, K. Hirose, T. Ohtsuki, Y. Watanabe, Y. Aritomo, and S. Hofmann, Phys. Rev. C **82**, 044604 (2010).

[32] T. Sikkeland, A. Ghiorso, and M. J. Nurmia, Phys. Rev. **172**, 1232 (1968).

[33] K. Eskola, P. Eskola, M. Nurmia, and A. Ghiorso, Phys. Rev. C **4**, 632 (1971).